JACS
JOURNAL OF THE AMERICAN CHEMICAL SOCIETY
pubs.acs.org/JACS
Article

Mitochondria-Targeting Type-I Photodrug: Harnessing Caspase-3 Activity for Pyroptotic Oncotherapy

Zhigao Yi,[§] Xujuan Qin,[§] Li Zhang,[§] Huan Chen,[§] Tianlin Song, Zichao Luo, Tao Wang, Junwei Lau, Yelin Wu, Tan Boon Toh, Chun-Sing Lee,* Wenbo Bu,* and Xiaogang Liu*

Cite This: *J. Am. Chem. Soc.* 2024, 146, 9413–9421

Read Online

ACCESS | Metrics & More | Article Recommendations | Supporting Information

ABSTRACT: Precise control of cellular signaling events during programmed cell death is crucial yet challenging for cancer therapy. The modulation of signal transduction in cancer cells holds promise but is limited by the lack of efficient, biocompatible, and spatiotemporally controllable approaches. Here we report a photodynamic strategy that modulates both apoptotic and pyroptotic cell death by altering caspase-3 protein activity and the associated signaling crosstalk. This strategy employs a mitochondria-targeting, near-infrared activatable probe (termed M-TOP) that functions via a type-I photochemical mechanism. M-TOP is less dependent on oxygen and more effective in treating drug-resistant cancer cells, even under hypoxic conditions. Our study shows that higher doses of M-TOP induce pyroptotic cell death via the caspase-3/gasdermin-E pathway, whereas lower doses lead to apoptosis. This photodynamic method is effective across diverse gasdermin-E-expressing cancer cells. Moreover, the M-TOP mediated shift from apoptotic to pyroptotic modulation can evoke a controlled inflammatory response, leading to a robust yet balanced immune reaction. This effectively inhibits both distal tumor growth and postsurgical tumor recurrence. This work demonstrates the feasibility of modulating intracellular signaling through the rational design of photodynamic anticancer drugs.

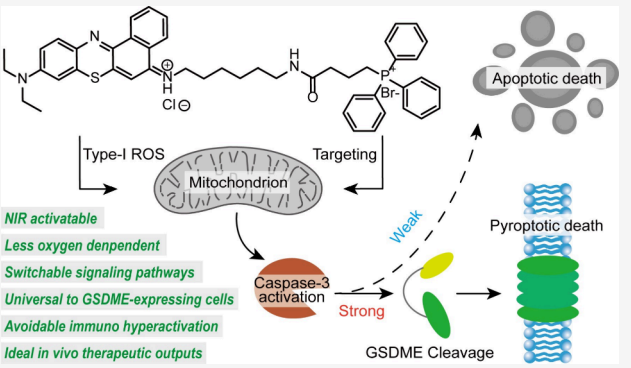

INTRODUCTION

Understanding and manipulating cellular signaling crosstalk during programmed cell death is critical for developing targeted therapies against diseases such as cancer and inflammatory disorders.[1−4] Apoptosis and pyroptosis, two distinct forms of programmed cell death, are essential for tissue homeostasis, immune response, and infection defense.[5−10] For example, pyroptosis triggers the release of pro-inflammatory cytokines such as IL-1β and IL-18, which can impact the apoptotic process by modulating the activity of apoptotic regulators and initiating an immune response that attracts immune cells to the cell death site. Although this inflammatory reaction intends to boost immune response against cancer cells or pathogens, excessive immune activation can lead to adverse effects.[11−13] Therefore, it is particularly important to balance inflammation-induced immunotherapeutic benefits with the risks of immune-related adverse events. The interplay between noninflammatory apoptosis and pro-inflammatory pyroptosis offers a therapeutic window due to their complex interactions, such as caspase protein activation. Caspases are a set of protease enzymes that play a vital role in cellular regulatory networks, controlling functions such as inflammation and programmed cell death. Apoptosis is primarily mediated by caspase-3/-7 activation, while canonical pyroptosis involves caspase-1/-4/-5/-11.[14,15] Recent findings also show caspase-3 mediated pyroptotic cancer cell death via gasdermin-E (GSDME) activation, linking the apoptotic and pyroptotic pathways.[16−18] Therefore, manipulating caspase-3 activity could be a feasible strategy to achieve effective therapy with minimal systemic side effects.

Caspase-3, an executioner caspase, cleaves various intracellular proteins, including structural proteins such as actin and lamin, DNA repair proteins such as PARP (poly ADP-ribose polymerase), cytoskeletal proteins such as fodrin, and signaling proteins such as ROCK (Rho-associated protein kinase). This breakdown ultimately leads to degradation of cellular components and cell degradation. Its translocation from the cytoplasm into mitochondria triggers apoptotic signal amplification, associated with permeabilization of the outer membrane of the mitochondrial and the release of pro-apoptotic factors such as cytochrome c.[19,20] Moreover,

Received: February 6, 2024
Revised: February 29, 2024
Accepted: March 8, 2024
Published: March 20, 2024

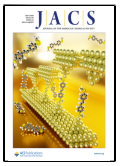

https://doi.org/10.1021/jacs.4c01929
J. Am. Chem. Soc. 2024, 146, 9413−9421

mitochondrial dysfunction can trigger a pyroptotic cascade by activating the NLRP3 inflammasome, releasing DAMPs, and initiating caspase-mediated pathways.[21−24] Taken together, the control of mitochondrial dynamics such as fission, fusion, and movement within cells may affect caspase-3 activity and subsequently modulate cell fate via either apoptotic or pyroptotic pathways.

Photodynamic interventions, known for their spatial and temporal precision in cancer treatment, take advantages of reactive oxygen species generation by photosensitizers.[25−29] Unlike the type-II pathway under energy transfer mechanism, type-I photosensitizers generate cytotoxic radicals (e.g., $O_2^{-\bullet}$) via electron transfer, making them suitable for oxygen-deprived environments like solid tumors.[30−33] Nile blue derivatives, recognized as outstanding type-I photodrugs with near-infrared light excitability and high radical productivity, can be modified for targeting.[34−37] We reasoned that apoptotic and pyroptotic cell deaths could be spatiotemporally modulated by a mitochondria-targeting photodrug (Figure 1a). In our design,

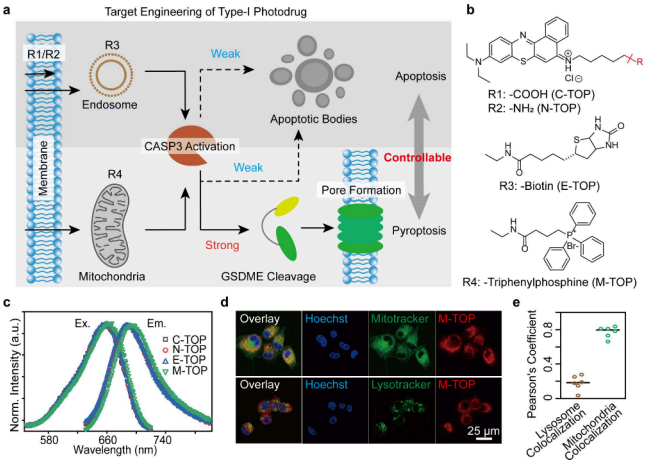

Figure 1. Harnessing caspase-3 activity enabled by mitochondrial-targeting type-I photodrugs. (a) Illustration of photodrug mechanism. This scheme provides an overview of the photodrug's design, focusing on its organelle-targeting capabilities and interaction with caspase-3. It highlights how direct interaction between the photodrug and mitochondria activates caspase-3, leading to the formation of pyroptotic pores in cell membrane via the GSDME-mediated pathway. In contrast, indirect interactions are shown to more gently activate caspase-3, resulting in the formation of apoptotic bodies indicative of apoptosis. (b) Chemical structures of photodrugs. (c) Excitation (Ex.) and emission (Em.) profiles of the photodrugs under investigation. (d and e) Colocalization and the corresponding Pearson's correlation efficient of M-TOP (red) with mitochondria or lysosomes (green) after 30 min of incubation with cells, respectively.

we combined a mitochondrial targeting segment, triphenylphosphine, with type-I photodrug nile-blue analogues (termed M-TOP, Figure 1b). We assessed the signaling pathway modulation and phototherapeutic effects of M-TOP compared to those of other targeting endosomes (E-TOP) and membranes (C-TOP and N-TOP). We also defined key parameters for switching between apoptotic and pyroptotic cell deaths. Our findings show that the M-TOP-mediated pyroptotic strategy is applicable to various GSDME-expressing cancer cells, with promising immunotherapeutic performance in *in situ*, distal, and recurrent xenograft tumor models.

RESULTS AND DISCUSSION

The purity of all synthetic photodrugs and their intermediates was confirmed by nuclear magnetic resonance and time-of-flight mass spectrometry (Methods in the Supporting Information, Figures S1−S15). Each photodrug exhibited a near-infrared absorption band at 660 nm and an emission band at 700 nm (Figure 1c). Theoretical investigations based on frontier molecular orbital distribution, energy calculations, and spin−orbit coupling matrix element assessments showed negligible perturbation after terminal group functionalization (Figure S16). These results support the suitabilities of these photodrugs as potential near-infrared activatable photodynamic probes.

To verify the effectiveness of our oncotherapeutic approach, which combines type-I photodynamics with signaling crosstalk modulation, we performed cellular experiments using the chemodrug-resistant human glioblastoma U251-MG cell line (Figure S17).[38−40] Subcellular colocalization analysis compared the targeting functionalized photodrugs against standard lysotracker and mitotracker. Confocal fluorescence microscopy revealed that M-TOP overlapped with mitochondria, E-TOP with endosomes/lysosomes, and C-TOP/N-TOP showed nonspecific targeting (Figure 1d,e and Figure S18). The generation of peroxygen radicals, rather than singlet oxygen, by these photodrugs under 640 nm irradiation was confirmed in both solutions and living cells (Figure 2a and Figure S19), consistent with previous studies on nile-blue derivatives.[34−37] The photodrugs exhibited time- and dosage-dependent increases in cellular uptake, as quantified through confocal imaging and flow cytometry (Figures S20 and S21). Intracellular dynamics showed maximal concentrations of photodrugs in cells after 30 min of incubation.

Cells treated with M-TOP and exposed to light showed morphological changes, including shrinkage and large bubble formation on the cell membrane after 3 h of incubation, indicative of pyroptotic cell death (Figure 2b). This process involves the activation and aggregation of certain gasdermin proteins on the membrane, leading to pore formation, influx of extracellular water, and leakage of cytoplasmic contents such as enzymes and cytokines.[5−10] Cell damage was further confirmed by monitoring lactate dehydrogenase (LDH) and interleukin-1 beta (IL-1β) in culture media. The M-TOP treated group showed a dosage-dependent increase in these markers, while no significant release was observed with other photodrug treatments (Figure 2c). Taken together, cell death and pyroptotic characteristics, such as pore formation and LDH/IL-1β release, occurred only in the M-TOP treated group. This highlights the critical role of mitochondria-targeting functionalization in enhancing photodynamic anticancer effects via a certain pyroptotic pathway.

The molecular mechanism of signaling transduction was further confirmed using Western blotting assay (Figure 2d). M-TOP phototreatment induced peroxygen radicals, which affected the mitochondrial respiratory chain and triggered the release of cytochrome C. This interaction with mitochondria activated caspase-3, as evidenced by a decrease in full-length caspase-3 and an increase in cleaved caspase-3 expression. This activation led to both apoptotic and pyroptotic pathways, as indicated by the presence of cleaved poly-ADP ribose polymerase (PARP) and cleaved gasdermin-E. However, only morphological changes were observed in the M-TOP photo-treated group (Figure 2b), suggesting that pyroptosis transmits

https://doi.org/10.1021/jacs.4c01929
J. Am. Chem. Soc. 2024, 146, 9413−9421

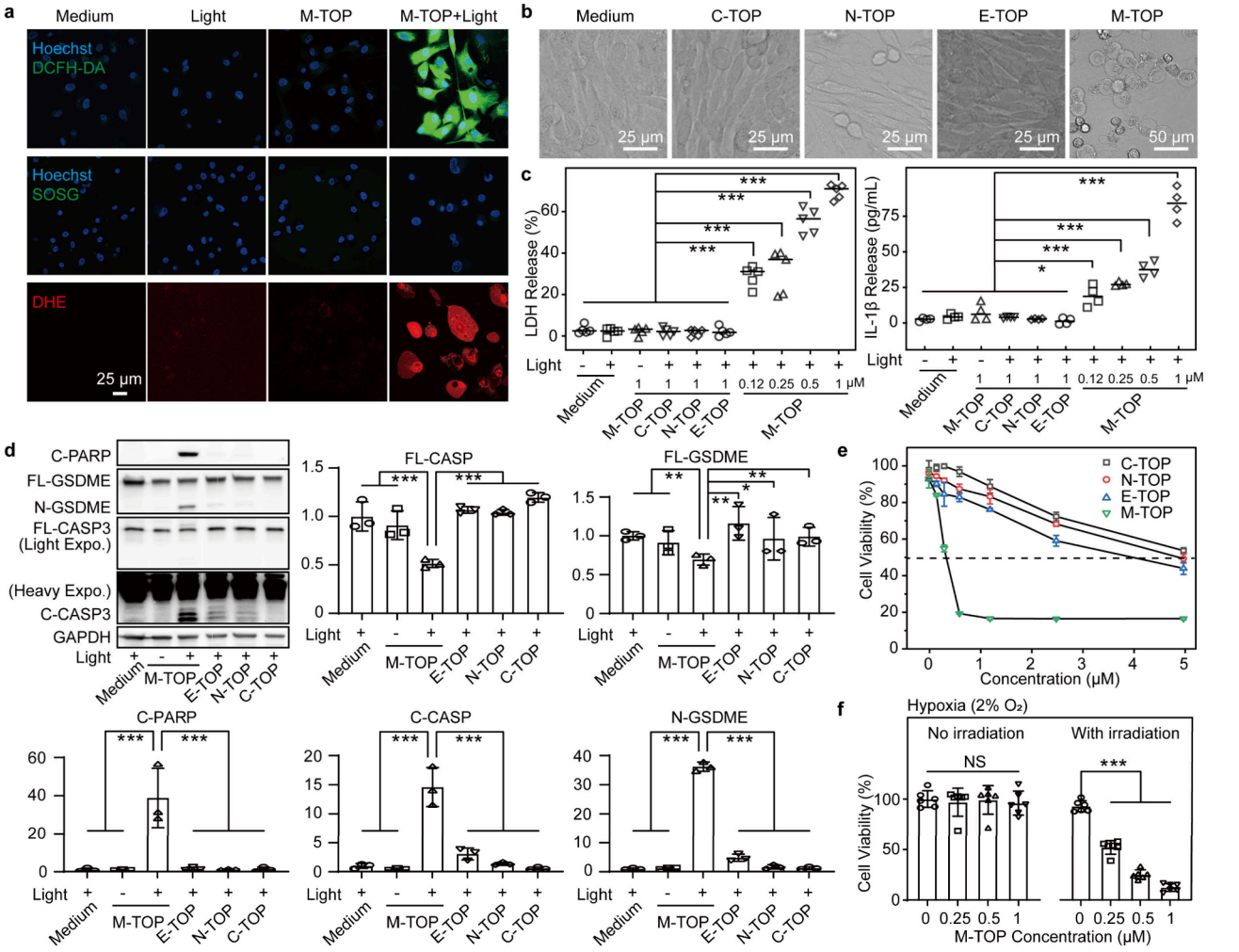

Figure 2. Photodynamic effects of mitochondrial-targeting type-I photodrug on apoptotic and pyroptotic deaths in U251-MG cells. (a) Identification of ROS generation using specific indicators: DCFH-DA for general ROS, SOSG for singlet oxygen, and DHE for reactive radicals. (b and e) Morphological changes assessed by phase-contrast imaging, LDH/IL-1β release profile, Western blot assays, and cell viability curves after photodrug treatment (1 μM dosage, 5 min irradiation at 15 mW/cm^2, 3 h incubation), respectively. Abbreviations: exposure (Expo.); full length (FL); no significance (NS). (f) Cell viability tests showing the benefits of M-TOP treatment in terms of biosafety and less oxygen-dependence. All data are representative of at least three independent experiments. The statistical data are presented as the mean ± s.d. and analyzed using one-way ANOVA and Tukey's tests. *p < 0.05, **p < 0.01, ***p < 0.001

signals more rapidly than apoptosis.[16] This was supported by MTT assays, where the M-TOP phototreament resulted in significantly reduced cell viability within a short period (Figure 2e). To assess the efficacy of type-I photochemistry under anticancer conditions, cells were cultured under a lower oxygen condition (2 vt% O_2) to simulate hypoxia in solid tumors (Figure S22). Even under hypoxia conditions, M-TOP maintained its superior cancer-cell killing performance, as confirmed by cell viability results (Figure 2f).

The modulation of caspase-3 signaling between non-inflammatory apoptosis and pro-inflammatory pyroptosis could prevent immune hyperactivation and associated adverse effects in immunotherapy. Most U251-MG cells underwent apoptotic death under a low dose of M-TOP (0.25 μM) with 5−10 min of irradiation (Figure 3a−d). In contrast, a higher M-TOP dose (1 μM) for 5 min of irradiation predominantly induced pyroptotic death (Figure 3e−h). The threshold for switching from apoptosis to pyroptosis was determined to be 0.5 μM dosage and 5 min of 640 nm irradiation at 15 mW/cm^2. This signaling switch correlated to the activation level of caspase-3, consistent with the expression levels of full-length caspase-3 (Figure 3c,g). This type-I pyroptotic oncotherapy strategy was also verified on various human and mouse cancer cell lines. All cell types, except for MCF-7 cells, exhibited membrane swelling and bubbling formation following M-TOP phototreatment with defined critical parameters (Figure 3j). Subsequent analysis of GSDME expression in these cell lines linked it to M-TOP-mediated pyroptosis. It is important to note that pyroptosis-mediated cancer cell death is beneficial for inducing an antitumor immune response.[5−10] Considering the pivotal role of dendritic cell activation in immunotherapy, where it initiates and coordinates the immune response against cancer cells, we proceeded to incubate mouse dendrite cells (DC2.4 cells) with supernatants from M-TOP phototreated cancer cells. Flow cytometry evaluation showed a significant enhancement in dendrite cell maturation and the release of inflammatory cytokines. This suggests the potential of M-TOP-mediated pyroptotic cancer death in activating an immune response (Figure S23).

https://doi.org/10.1021/jacs.4c01929
J. Am. Chem. Soc. 2024, 146, 9413−9421

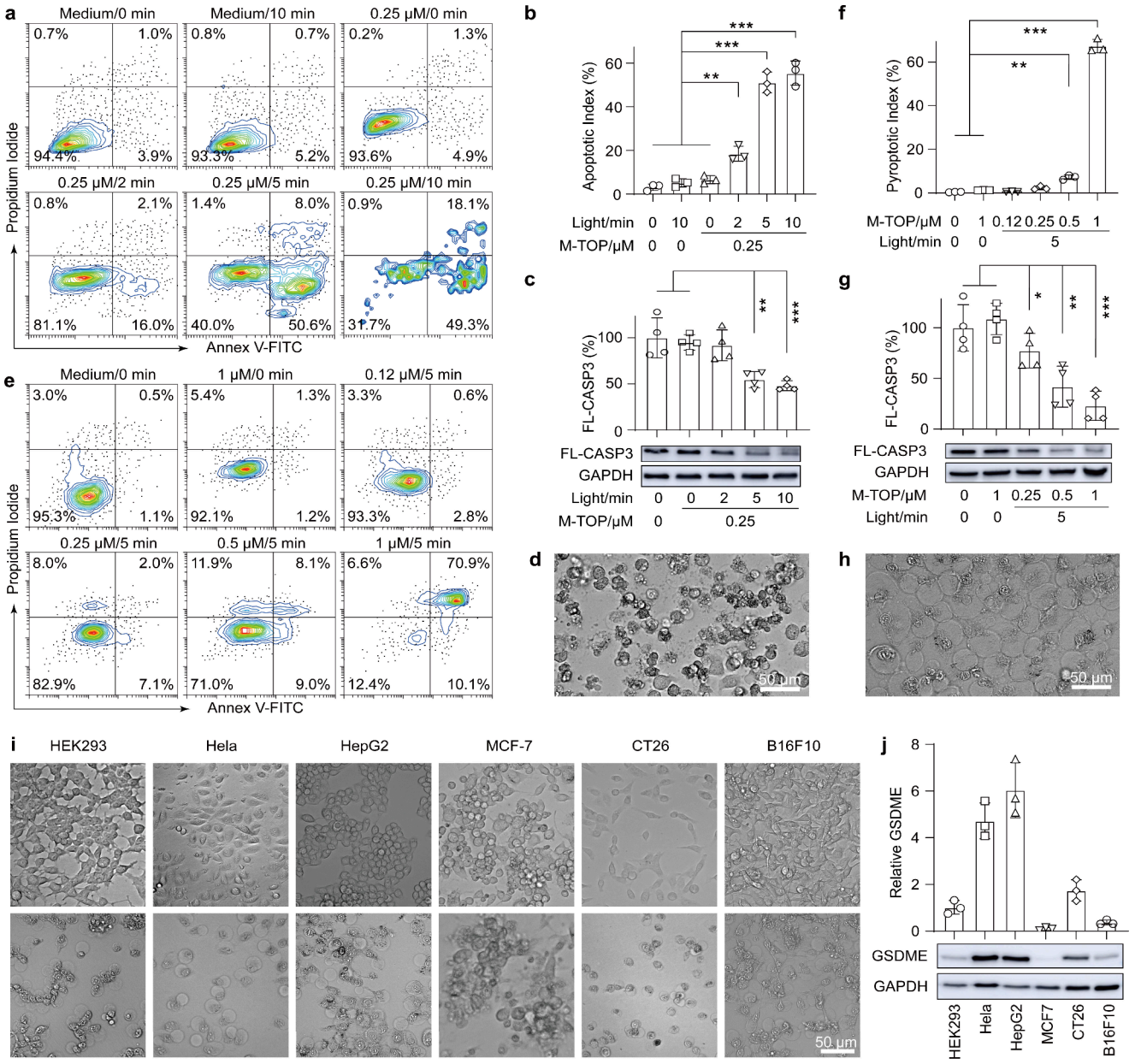

Figure 3. Identification of caspase-3 activity in M-TOP mediated cell death and the reproducible paradigm in various cancer cell lines. (a–d) Irradiation-dependent cell death observed over a 24 h incubation period, as determined by flow cytometry assays (a), statistical analysis of propidium iodide- and annexin V-fluorescein isothiocyanate (FITC)-stained cells (b), Western blotting assays showing relatively weak activation of caspase-3 (c), and phase-contrast imaging (d) showing dominant apoptotic morphological changes after M-TOP phototreatment (0.25 μM, 10 min irradiation). (e–h) Administration dosage dependent cell death over a 3 h incubation period, as determined by flow cytometry assays (e), statistical analysis (f), Western blotting assays showing a relatively strong activation of caspase-3 (g), and phase-contrast imaging (h) showing dominant pyroptotic morphological change after M-TOP phototreatment (1 μM, 5 min irradiation). (i and j) Expanded investigation in various cancer cell lines. (i) Phase-contrast images showing morphological change after M-TOP administration (1 μM, 5 min of irradiation, 3 h of incubation). (j) Corresponding Western blotting assays that show the expression level of GSDME in each cell line. All data are representative of at least three independent experiments. Statistical data in panels b, c, f, and g are presented as mean ± s.d. and analyzed using one-way ANOVA and Tukey's tests. *$p < 0.05$, **$p < 0.01$, ***$p < 0.001$.

Given the promising *in vitro* findings that demonstrate anticancer activity and activation of dendritic cells (DCs), we hypothesized that M-TOP phototreatment could enhance the cancer-immunity cycle.[41] This enhancement is expected to involve DC maturation, antigen presentation, T-cell priming, and the induction of immunogenic cell death in tumors. We conducted a systematic *in vivo* efficacy study against malignant solid tumors using a subcutaneous xenograft carcinoma model (Figure 4a). Compared to the control groups (PBS, Light, or M-TOP), the M-TOP phototreatment group (M-TOP+Light) showed superior tumor suppression, including complete tumor regression ($n = 8$), as measured by tumor weight, volume, and survival rate (Figure 4b–e).

Further analysis of tumor tissues from the M-TOP+Light group revealed insights into the tumor microenvironment. Flow cytometry of single-cell suspensions showed an increased infiltration of $CD4^+$ and $CD8^+$ T cells, suggesting enhanced immune activation (Figure 4f). Specifically, the increase in

https://doi.org/10.1021/jacs.4c01929
J. Am. Chem. Soc. 2024, 146, 9413–9421

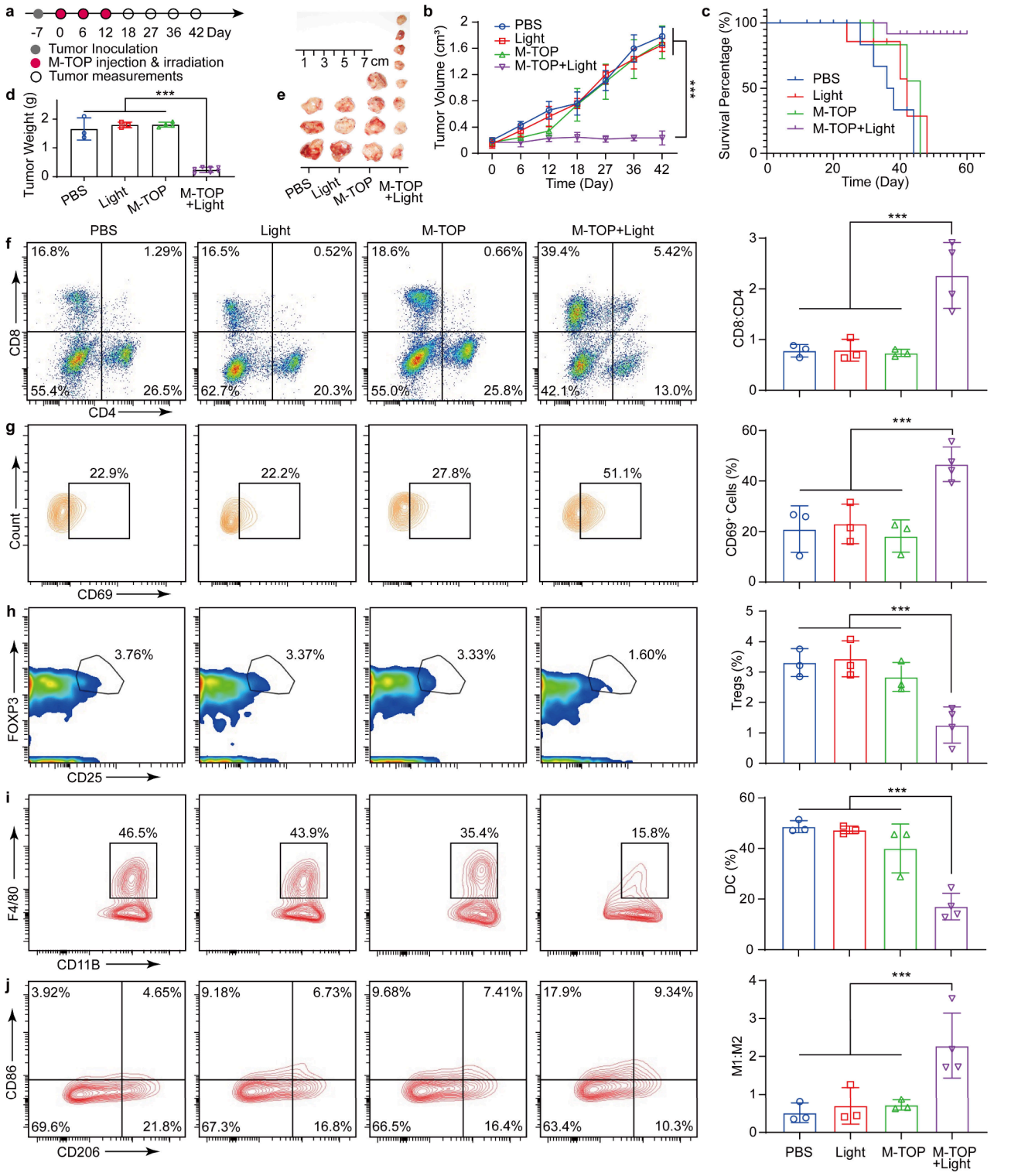

Figure 4. Immunotherapeutic performance of M-TOP phototreatment against primary tumor-bearing animal models. (a) Schedule for the establishment of the primary tumor-bearing model, phototreatment, and tumor measurements (n = 8 mice per group), (b and c) Monitoring of tumor volume and survival ratio, respectively, during treatment (log-rank test for panel (c), n = 6 replicates per group, M-TOP+Light vs control groups including PBS, Light, and M-TOP, respectively). (d and e) Tumor weight statistics and the corresponding photographs, respectively, after treatment. (f–j) Flow cytometry assays and the corresponding statistic quantification showing (f) $CD4^+$ and $CD8^+$ T cells, (g) $CD69^+$ activated T cells, (h and i) Treg and macrophage cells in tumors, and (j) M1 $CD86^+$ and M2 $CDCD206^+$ macrophages (n = 3 or 4 replicates per group). The flow gate strategies for parts f–j are shown in Figure S25. Statistical data are presented as mean ± s.d. and analyzed using two-tailed student's t test for panel b and one-way ANOVA with Tukey's tests for panels d and f–j. ***$p < 0.001$.

$CD8^+$ cytotoxic T lymphocytes and $CD4^+$ helper T lymphocytes suggests a potential boost in antitumor cellular immunity. Notably, the population of activated $CD8^+$ T cells ($CD8^+CD69^+$) was more than double that in the control

https://doi.org/10.1021/jacs.4c01929
J. Am. Chem. Soc. 2024, 146, 9413–9421

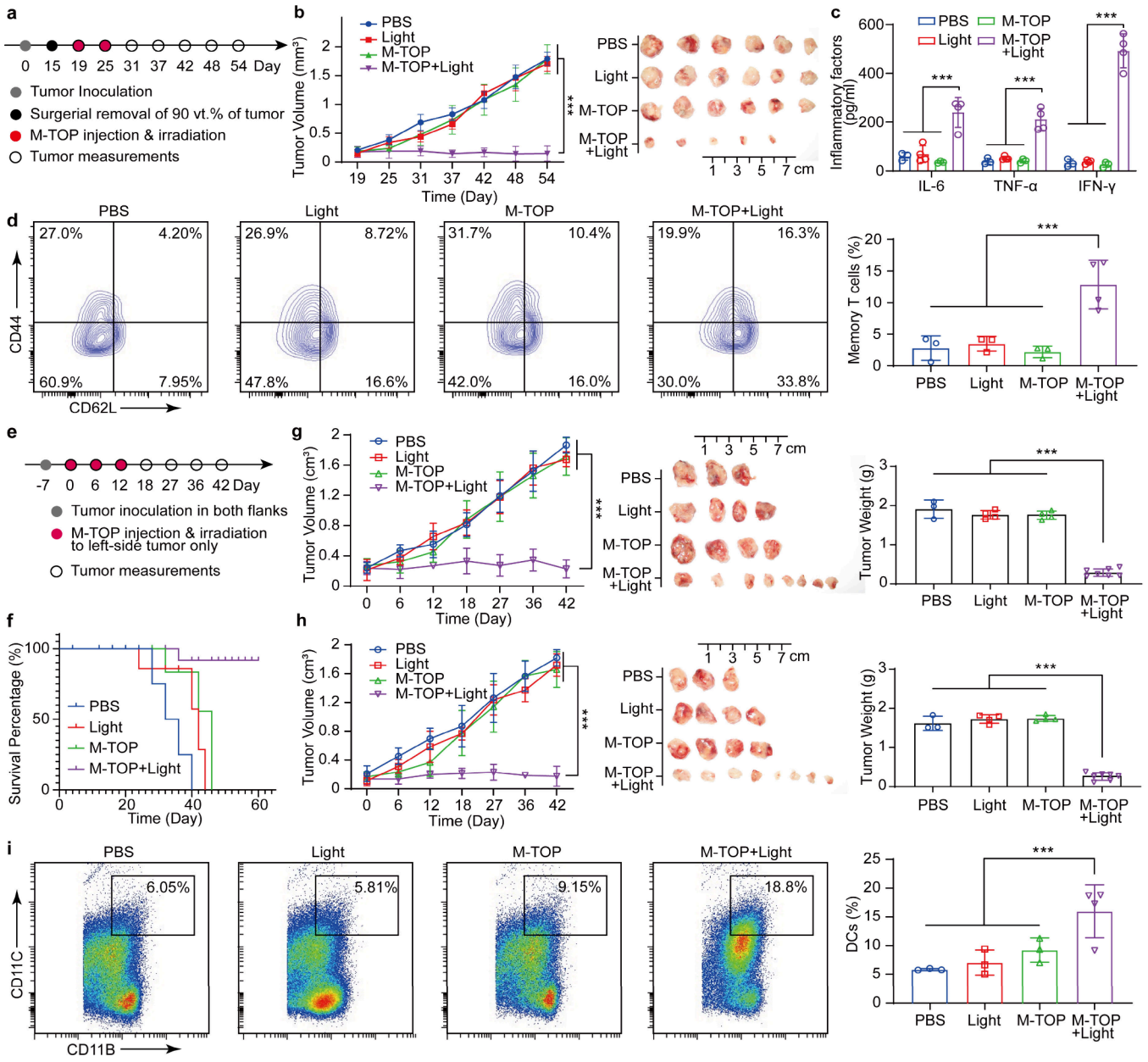

Figure 5. Antitumor effect of M-TOP phototreatment against distal and recurrence tumors in animal models. (a) Schedule for establishment of the recurrence tumor model, phototreatment, and tumor measurements (n = 6 mice per group). (b) Tumor volume measurements during treatment and the photograph record after treatment. (c) Release of IL-6, TNF-α, and IFN-γ cytokines in serum. (d) Flow cytometry assays and the corresponding statistics showing $CD44^+CD62L^+$ effector memory T cells in tumors. (e) Timing of distal tumor model establishment, phototreatment procedures, and tumor measurements (n = 8 mice per group). (f) Survival percentage of tumor-bearing mice during treatment (log-rank test, n = 6 replicates per group, M-TOP+Light vs control groups including PBS, Light, and M-TOP, respectively). (g and h) Tumor measurement including volume, photograph, and weight of (g) primary and (h) distal tumors during and after treatment, respectively. (i) Flow cytometry assays and the corresponding statistics showing DC Treg cells in distal tumors. The flow gate strategies for panels d and i are shown in Figure S26 (n = 3 or 4 replicates per group for panels d and i). Their statistical data are presented as the mean ± s.d. and analyzed using one-way ANOVA and Tukey's tests, expect for two-tailed student's t test for tumor volumes comparisons in panels b, g, and h. ***$p < 0.001$.

groups, underscoring the role of T lymphocyte activation *in vivo* (Figure 4g). The M-TOP+Light group also showed almost complete elimination of immunosuppressive T lymphocytes (Tregs) within the tumor microenvironment, in contrast to the control groups (Figure 4h). Moreover, there was a marked increase in mature DCs, which are essential for initiating antitumor immunity (Figure 4i), and a significant decrease in M2-type macrophages, which often support tumor growth (Figure 4j).[42,43]

We next investigated M-TOP phototreatment in a tumor recurrence model, as recurrences are often more frequent and malignant and pose a challenge to conventional oncotherapies (Figure 5a).[44] Over a 54-day observation period, M-TOP phototreatment effectively suppressed malignant tumor recurrence with no deaths, unlike that in the control groups (Figure 5b). This was supported by the notable increase in effector memory T cells ($CD44^+CD62L^+$) in the M-TOP +Light group, which is essential for recognizing and preventing tumor recurrence (Figure 5c). Considering the clinical

https://doi.org/10.1021/jacs.4c01929
J. Am. Chem. Soc. 2024, 146, 9413−9421

challenge of distant tumor metastasis,[45] we evaluated the distant effect of M-TOP phototreatment using subcutaneous xenograft tumor models with tumor cells implanted in both flanks of mice (Figure 5d). The survival benefit in the M-TOP +Light group was significantly longer than that in the control groups (Figure 5e), with both primary and distal tumor growth inhibited (Figure 5f,g). The abscopal effects in distal tumors were marked by an enrichment of mature DCs (Figure 5h). Immunofluorescence staining of distal tumors also showed the presence of high mobility group box 1 (HMGB1) and calreticulin (CRT) in M-TOP+Light group (Figure S24), indicating an association with immunogenic cell death, a form of programmed cell death that triggers an immune response against dying cells.[46]

CONCLUSIONS

In this work, we have introduced a photodynamic strategy capable of efficiently modulating caspase-3 activity, a critical component in both apoptotic and pyroptotic signaling pathways. By utilizing a mitochondria-targeting molecular probe with a type-I photochemical mechanism, we have shown its therapeutic efficacy against drug-resistant cancer cells with the advantage of reduced reliance on oxygen. This approach allows for spatiotemporal control of inflammatory responses, thereby preventing excessive immune activation and emphasizing the need for balancing therapeutic efficacy with potential risks. These findings highlight the potential of M-TOP in cancer immunotherapy, with the aim of achieving therapeutic outcomes while minimizing systemic side effects (Table S2). This approach can act as a supplementary tool for clinical cancer therapies, including chemotherapy and radiotherapy, especially in cases of tumor metastasis and recurrence. This work presents an example of modulating signaling crosstalk with precision through photodynamic interventions, thereby expanding the range of tools available in molecular medicine and disease treatment.

ASSOCIATED CONTENT

Supporting Information

The Supporting Information is available free of charge at https://pubs.acs.org/doi/10.1021/jacs.4c01929.

Materials and methods; detailed experimental procedures; molecule characterizations; theoretical calculation; reactive oxygen species quantification; cell lines; cellular uptake and growth; flow cytometry; Western blot; MTT assay; animal models; in vitro immune activation, immunostaining; flow gate strategies; Figures S1−S25 and Tables S1 and S2 (PDF)

AUTHOR INFORMATION

Corresponding Authors

Chun-Sing Lee − *Center of Super-Diamond and Advanced Films (COSDAF), Department of Chemistry, City University of Hong Kong, Kowloon 999077, Hong Kong SAR, P. R. China;* orcid.org/0000-0001-6557-453X; Email: apcslee@cityu.edu.hk

Wenbo Bu − *Department of Materials Science, Fudan University, Shanghai 200438, P. R. China; Center for Biotechnology and Biomedical Engineering, Yiwu Research Institute of Fudan University, Yiwu 322000, P. R. China; Department of Medical Ultrasound, Shanghai Tenth People's Hospital, Tongji University Cancer Center, Tongji University School of Medicine, Shanghai 200072, P. R. China;* orcid.org/0000-0001-6664-3453; Email: wbbu@fudan.edu.cn

Xiaogang Liu − *Department of Chemistry, National University of Singapore, Singapore 117543, Singapore; The N1 Institute for Health, National University of Singapore, Singapore 117456, Singapore; Department of Surgery, Yong Loo Lin School of Medicine, National University of Singapore, Singapore 119228, Singapore;* orcid.org/0000-0003-2517-5790; Email: chmlx@nus.edu.sg

Authors

Zhigao Yi − *Department of Chemistry, National University of Singapore, Singapore 117543, Singapore; The N1 Institute for Health, National University of Singapore, Singapore 117456, Singapore;* orcid.org/0000-0003-0853-2055

Xujuan Qin − *Department of Materials Science, Fudan University, Shanghai 200438, P. R. China; Center for Biotechnology and Biomedical Engineering, Yiwu Research Institute of Fudan University, Yiwu 322000, P. R. China*

Li Zhang − *Department of Medical Ultrasound, Shanghai Tenth People's Hospital, Tongji University Cancer Center, Tongji University School of Medicine, Shanghai 200072, P. R. China*

Huan Chen − *Center of Super-Diamond and Advanced Films (COSDAF), Department of Chemistry, City University of Hong Kong, Kowloon 999077, Hong Kong SAR, P. R. China*

Tianlin Song − *Shanghai Key Laboratory of Regulatory Biology, Institute of Biomedical Sciences, School of Life Sciences, East China Normal University, Shanghai 200241, China*

Zichao Luo − *Department of Chemistry, National University of Singapore, Singapore 117543, Singapore; The N1 Institute for Health, National University of Singapore, Singapore 117456, Singapore*

Tao Wang − *Department of Chemistry, National University of Singapore, Singapore 117543, Singapore*

Junwei Lau − *Department of Chemistry, National University of Singapore, Singapore 117543, Singapore; The N1 Institute for Health, National University of Singapore, Singapore 117456, Singapore*

Yelin Wu − *Department of Medical Ultrasound, Shanghai Tenth People's Hospital, Tongji University Cancer Center, Tongji University School of Medicine, Shanghai 200072, P. R. China*

Tan Boon Toh − *The N1 Institute for Health, National University of Singapore, Singapore 117456, Singapore;* orcid.org/0000-0003-0292-6985

Complete contact information is available at: https://pubs.acs.org/10.1021/jacs.4c01929

Author Contributions

[§]These authors contributed equally.

Notes

The authors declare no competing financial interest.

ACKNOWLEDGMENTS

This work was supported by the National Research Foundation, Prime Minister's Office, Singapore, under its Competitive Research Program (award no. NRF-CRP23-2019-0002) and under its NRF Investigatorship Programme (award no. NRF-NRFI05-2019-0003), Key Program of National

Natural Science Foundation of China (#22235004), National Science Foundation for the Young Scientists of China (Grant No. 82202152), Postdoctoral Research Project of China (Grant No. 2022M712416), Innovation Program of Shanghai Municipal Education Commission (#2023ZKZD01), and the Research Grants Council of Hong Kong Special Administrative Region, General Research Fund (Project No. CityU 11300320 and 11318322). All animal experiments were conducted in compliance with the guidelines of the national law and rules and the animal protocol (#202203007S) approved by the Ethic Committee of Animal Care and Use of Fudan University.

REFERENCES

(1) Bedoui, S.; Herold, M. J.; Strasser, A. Emerging connectivity of programmed cell death pathways and its physiological implications. *Nat. Rev. Mol. Cell Biol.* **2020**, *21*, 678−695.
(2) Brown, J. M.; Attardi, L. D. The role of apoptosis in cancer development and treatment response. *Nat. Rev. Cancer* **2005**, *5*, 231−237.
(3) Jorgensen, I.; Rayamajhi, M.; Miao, E. Programmed cell death as a defence against infection. *Nat. Rev. Immunol.* **2017**, *17*, 151−164.
(4) Jiang, M.; Qi, L.; Li, L.; Li, Y. The caspase-3/GSDME signal pathway as a switch between apoptosis and pyroptosis in cancer. *Cell Death Discovery* **2020**, *6*, 112.
(5) Carneiro, B. A.; El-Deiry, W. S. Targeting apoptosis in cancer therapy. *Nat. Rev. Clin. Oncol.* **2020**, *17*, 395−417.
(6) Minton, K. Pyroptosis heats tumour immunity. *Nat. Rev. Immunol.* **2020**, *20*, 274−275.
(7) Xia, X.; Wang, X.; Cheng, Z.; Qin, W.; Lei, L.; Jiang, J.; Hu, J. H. The role of pyroptosis in cancer: pro-cancer or pro-"host"? *Cell Death Discovery* **2019**, *10*, 650.
(8) Wang, Q.; Wang, Y.; Ding, J.; Wang, C.; Zhou, X.; Gao, W.; Huang, H.; Shao, F.; Liu, Z. A bioorthogonal system reveals antitumour immune function of pyroptosis. *Nature* **2020**, *579*, 421−426.
(9) Wang, N.; Liu, C.; Li, Y.; Huang, D.; Wu, X.; Kou, X.; Wang, X.; Wu, Q.; Gong, C. A cooperative nano-CRISPR scaffold potentiates immunotherapy via activation of tumour-intrinsic pyroptosis. *Nat. Commun.* **2023**, *14*, 779.
(10) Cong, L.; Bai, Y.; Guo, Z. The crosstalk among autophagy, apoptosis, and pyroptosis in cardiovascular disease. *Front. Cardiovasc. Med.* **2022**, *9*, No. 997469.
(11) O'Sullivan, D.; Sanin, D. E.; Pearce, E. J.; Pearce, E. L. Metabolic interventions in the immune response to cancer. *Nat. Rev. Immunol.* **2019**, *19*, 324−335.
(12) Pan, W.; Wang, Q.; Chen, Q. The cytokine network involved in the host immune response to periodontitis. *Int. J. Oral Sci.* **2019**, *11*, 30.
(13) Diamond, M. S.; Kanneganti, T. D. Innate immunity: the first line of defense against SARS-CoV-2. *Nat. Immunol.* **2022**, *23*, 165−176.
(14) Fitzgerald, M. C.; O'Halloran, P. J.; Connolly, N. M. C.; Murphy, B. M. Targeting the apoptosis pathway to treat tumours of the paediatric nervous system. *Cell Death Discovery* **2022**, *13*, 460.
(15) Shen, S.; Shao, Y.; Li, C. Different types of cell death and their shift in shaping disease. *Cell Death Discovery* **2023**, *9*, 284.
(16) Wang, Y.; Gao, W.; Shi, X.; Ding, J.; Liu, W.; He, H.; Wang, K.; Shao, F. Chemotherapy drugs induce pyroptosis through caspase-3 cleavage of a gasdermin. *Nature* **2017**, *547*, 99−103.
(17) Zhang, Z.; Zhang, Y.; Xia, S.; Kong, Q.; Li, S.; Liu, X.; Junqueira, C.; Meza-Sosa, K. F.; Mok, T. M. Y.; Ansara, J.; Sengupta, S.; Yao, Y.; Wu, H.; Lieberman, J. Gasdermin E suppresses tumour growth by activating anti-tumour immunity. *Nature* **2020**, *579*, 415−420.
(18) Yu, J.; Li, S.; Qi, J.; Chen, Z.; Wu, Y.; Guo, J.; Wang, K.; Sun, X.; Zheng, J. Cleavage of GSDME by caspase-3 determines lobaplatin-induced pyroptosis in colon cancer cells. *Cell Death Discovery* **2019**, *10*, 193.
(19) Porter, A. G.; Janicke, R. U. Emerging roles of caspase-3 in apoptosis. *Cell Death Differ.* **1999**, *6*, 99−104.
(20) Rogers, C.; Erkes, D. A.; Nardone, A.; Aplin, A. E.; Fernandes-Alnemri, T.; Alnemri, E. S. Gasdermin pores permeabilize mitochondria to augment caspase-3 activation during apoptosis and inflammasome activation. *Nat. Commun.* **2019**, *10*, 1689.
(21) Weindel, C. G.; Martinez, E. L.; Zhao, X.; Mabry, C. J.; Bell, S. L.; Vail, K. J.; Coleman, A. K.; VanPortfliet, J. J.; Zhao, B.; Wagner, A. R.; Azam, S.; Scott, H. M.; Li, P.; West, A. P.; Karpac, J.; Patrick, K. L.; Watson, R. O. Mitochondrial ROS promotes susceptibility to infection via gasdermin D-mediated necroptosis. *Cell* **2022**, *185*, 3214−3231.
(22) Zhang, Y.; Zhou, L.; Mao, H.; Yang, F.; Chen, Z.; Zhang, L. Mitochondrial DNA leakage exacerbates odontoblast inflammation through gasdermin D-mediated pyroptosis. *Cell Death Discovery* **2021**, *7*, 381.
(23) Nguyen, T. T.; Wei, S.; Nguyen, T. H.; Jo, Y.; Zhang, Y.; Park, W.; Gariani, K.; Oh, C.-M.; Kim, H. H.; Ha, K.-T.; Park, K. S.; Park, R.; Lee, I.-K.; Shong, M.; Houtkooper, R. H.; Ryu, D. Mitochondria-associated programmed cell death as a therapeutic target for age-related disease. *Exp. Mol. Med.* **2023**, *55*, 1595−1619.
(24) Shen, X.; Wang, H.; Weng, C.; Jiang, H.; Chen, J. Caspase 3/GSDME-dependent pyroptosis contributes to chemotherapy drug-induced nephrotoxicity. *Cell Death Discovery* **2021**, *12*, 186.
(25) Dolmans, D.; Fukumura, D.; Jain, R. Photodynamic therapy for cancer. *Nat. Rev. Cancer* **2003**, *3*, 380−387.
(26) Li, X.; Lovell, J. F.; Yoon, J.; Chen, X. Clinical development and potential of photothermal and photodynamic therapies for cancer. *Nat. Rev. Clin. Oncol.* **2020**, *17*, 657−674.
(27) Liu, J.; Bu, W.; Shi, J. Chemical design and synthesis of functionalized probes for imaging and treating tumor hypoxia. *Chem. Rev.* **2017**, *117*, 6160−6224.
(28) Pham, T. C.; Nguyen, V.-N.; Choi, Y.; Lee, S.; Yoon, J. Recent strategies to develop innovative photosensitizers for enhanced photodynamic therapy. *Chem. Rev.* **2021**, *121*, 13454−13619.
(29) Ryu, K. A.; Kaszuba, C. M.; Bissonnette, N. B.; Oslund, R. C.; Fadeyi, O. O. Interrogating biological systems using visible-light-powered catalysis. *Nat. Rev. Chem.* **2021**, *5*, 322−337.
(30) Chen, K.; He, P.; Wang, Z.; Tang, B. Z. A feasible strategy of fabricating type I photosensitizer for photodynamic therapy in cancer cells and pathogens. *ACS Nano* **2021**, *15*, 7735−7743.
(31) Li, M.; Xu, Y.; Peng, X.; Kim, J. S. From low to no O_2-dependent hypoxia photodynamic therapy (hPDT): a new perspective. *Acc. Chem. Res.* **2022**, *55*, 3253−3264.
(32) Li, M.; Kim, J.; Rha, H.; Son, S.; Levine, M. S.; Xu, Y.; Sessler, J. L.; Kim, J. S. Photon-Controlled Pyroptosis Activation (PhotoPyro): an emerging trigger for antitumor immune response. *J. Am. Chem. Soc.* **2023**, *145*, 6007−6023.
(33) Tian, J.; Li, B.; Zhang, F.; Yao, Z.; Song, W.; Tang, Y.; Ping, Y.; Liu, B. Activatable Type I photosensitizer with quenched photosensitization pre and post photodynamic therapy. *Angew. Chem., Int. Ed.* **2023**, *62*, No. e202307288.
(34) Lin, C. W.; Shulok, J. R.; Kirley, S. D.; Cincotta, L.; Foley, J. W. Lysosomal localization and mechanism of uptake of Nile blue photosensitizers in tumor cells. *Cancer Res.* **1991**, *51*, 2710−2719.
(35) Li, M.; Xiong, T.; Du, J.; Tian, R.; Xiao, M.; Guo, L.; Long, S.; Fan, J.; Sun, W.; Shao, K.; Song, X.; Foley, J. W.; Peng, X. Superoxide radical photogenerator with amplification effect: surmounting the Achilles' heels of photodynamic oncotherapy. *J. Am. Chem. Soc.* **2019**, *141*, 2695−2702.
(36) Li, M.; Shao, Y.; Kim, J. H.; Pu, Z.; Zhao, X.; Huang, H.; Xiong, T.; Kang, Y.; Li, G.; Shao, K.; Fan, J.; Foley, J. W.; Kim, J. S.; Peng, X. Unimolecular photodynamic O_2-economizer to overcome hypoxia resistance in phototherapeutics. *J. Am. Chem. Soc.* **2020**, *142*, 5380−5388.
(37) Li, M.; Gebremedhin, K. H.; Ma, D.; Pu, Z.; Xiong, T.; Xu, Y.; Kim, J. S.; Peng, X. Conditionally activatable photoredox catalysis in living systems. *J. Am. Chem. Soc.* **2022**, *144*, 163−173.

(38) Rabé, M.; Dumont, S.; Álvarez-Arenas, A.; Janati, H.; Belmonte-Beitia, J.; Calvo, G. F.; Thibault-Carpentier, C.; Séry, Q.; Chauvin, C.; Joalland, N.; Briand, F.; Blandin, S.; Scotet, E.; Pecqueur, C.; Clairambault, J.; Oliver, L.; Perez-Garcia, V.; Nadaradjane, A.; Cartron, P.-F.; Gratas, C.; Vallette, F. M. Identification of a transient state during the acquisition of Temozolomide resistance in glioblastoma. *Cell Death Discovery* **2020**, *11*, 19.
(39) Stritzelberger, J.; Distel, L.; Buslei, R.; Fietkau, R.; Putz, F. Acquired Temozolomide resistance in human glioblastoma cell line U251 is caused by mismatch repair deficiency and can be overcome by lomustine. *Clin. Transl. Oncol.* **2018**, *20*, 508−516.
(40) Tu, G. X. E.; Ho, Y. K.; Ng, Z. X.; Teo, K. J.; Yeo, T. T.; Too, H.-P. A facile and scalable in production non-viral gene engineered mesenchymal stem cells for effective suppression of Temozolomide-resistant (TMZR) glioblastoma growth. *Stem Cell Res. Ther.* **2020**, *11*, 391.
(41) Palucka, K.; Banchereau, J. Cancer immunotherapy via dendritic cells. *Nat. Rev. Cancer* **2012**, *12*, 265−277.
(42) Togashi, Y.; Shitara, K.; Nishikawa, H. Regulatory T cells in cancer immunosuppression - implications for anticancer therapy. *Nat. Rev. Clin. Oncol.* **2019**, *16*, 356−371.
(43) Duan, Z.; Luo, Y. Targeting macrophages in cancer immunotherapy. *Signal Transduct. Target Ther.* **2021**, *6*, 127.
(44) Fang, L.; Zhao, Z.; Wang, J.; Zhang, P.; Ding, Y.; Jiang, Y.; Wang, D.; Li, Y. Engineering autologous tumor cell vaccine to locally mobilize antitumor immunity in tumor surgical bed. *Sci. Adv.* **2020**, *6*, No. eaba4024.
(45) Waldman, A. D.; Fritz, J. M.; Lenardo, M. J. A guide to cancer immunotherapy: from T cell basic science to clinical practice. *Nat. Rev. Immunol.* **2020**, *20*, 651−668.
(46) Stoetzer, O. J.; Fersching, D. M. I.; Salat, C.; Steinkohl, O.; Gabka, C. J.; Hamann, U.; Braun, M.; Feller, A.-M.; Heinemann, V.; Siegele, B.; Nagel, D.; Holdenrieder, S. Circulating immunogenic cell death biomarkers HMGB1 and RAGE in breast cancer patients during neoadjuvant chemotherapy. *Tumour Biol.* **2013**, *34*, 81−90.

https://doi.org/10.1021/jacs.4c01929
J. Am. Chem. Soc. 2024, 146, 9413−9421